

Nonlinear co-existence of beta-induced Alfvén eigenmodes and beta-induced Alfvén-acoustic eigenmodes

Junyi Cheng,^{1,2,3} Wenlu Zhang,^{1,2,3,4,a)} Zhihong Lin,^{4,5} Ding Li,^{1,2,3} Chao Dong,^{2,3} and Jintao Cao^{2,3}

¹Department of Modern Physics, University of Science and Technology of China, Hefei, Anhui 230026, China

²Beijing National Laboratory for Condensed Matter Physics and CAS Key Laboratory of Soft Matter Physics, Institute of Physics, Chinese Academy of Sciences, Beijing 100190, China

³University of Chinese Academy of Sciences, Beijing 100049, China

⁴Department of Physics and Astronomy, University of California, Irvine, California 92697, USA

⁵Fusion Simulation Center, Peking University, Beijing 100871, China

(Received 21 April 2017; accepted 13 September 2017; published online 28 September 2017)

The nonlinear co-existence of β -induced Alfvén eigenmode (BAE) and β -induced Alfvén-acoustic eigenmode (BAAE) is found in simulations using the gyrokinetic toroidal code, which provides a new mechanism responsible for BAAE excitation in tokamaks. Here, the normalized pressure β is the ratio between plasma thermal pressure and magnetic pressure. The nonlinear simulation results show that the BAAE branch emerges after the BAE branch is saturated. The mode structure's evolution shows that existence of BAAE will change the original BAE mode structure. The perturbed distribution functions in the velocity phase space show that a new resonance region manifesting the wave-particle resonance in the BAAE branch appears during the nonlinear co-existence stage. Published by AIP Publishing. <https://doi.org/10.1063/1.5004676>

I. INTRODUCTION

Energetic particles, including fast ions and fast electrons produced by the fusion reaction and auxiliary heating, can excite various Alfvén instabilities in magnetic confinement fusion plasma such as toroidicity-induced Alfvén eigenmode (TAE),¹ β -induced Alfvén eigenmode (BAE),^{2,3} reversed shear Alfvén eigenmode (RASE),^{4,5} and β -induced Alfvén-acoustic eigenmode (BAAE),^{6,7} which may induce significant transport and degrade the overall plasma confinement.^{8–10} Here, the normalized pressure β is the ratio between plasma thermal pressure and magnetic pressure. The BAE is formed by finite compressibility induced by the geodesic curvature of equilibrium magnetic field and plasma pressure.^{11–13} The weakly-damped BAE has been widely observed in DIII-D,² TFTR,¹⁴ FTU,¹⁵ HL-2A,¹⁶ and Tore-Supra,¹⁷ and has been investigated by simulations using various codes, such as the gyrokinetic toroidal code (GTC),¹⁸ the MHD-gyrokinetic hybrid code (XHMGC)¹⁹ and the particle/MHD hybrid code (M3D).²⁰ The Alfvén instabilities related to fast electrons were widely observed, such as the internal kink mode and fishbone in DIII-D,²¹ BAE and fishbone in HL-2A.^{22,23} The fast-electron driven BAE was identified for the first time both in Ohmic and electron cyclotron resonance heating plasma in HL-2A^{23,24} and has been verified in linear simulations²⁵ using GTC. The BAAE is formed through the coupling of the shear Alfvén continuum and the acoustic continuum in the toroidal geometry, which was first formulated based on the magneto-hydrodynamics (MHD) approach.^{6,7} BAAE is then derived through kinetic theory.²⁶ Recently, the formulation of BAAE²⁷ is retained by solving the radial envelope equation in the ballooning mode theory taking into account kinetic

effects of thermal plasmas. BAAE has then been observed in various tokamaks such as DIII-D,²⁶ JET,^{6,7} NSTX,²⁸ and ASDEX²⁹ tokamak, and LHD,³⁰ HSX,³¹ and H1³² stellarators. And BAAE in toroidal plasmas is verified and studied by gyrokinetic particle simulations.^{33,34}

The frequency of BAAE is lower than the frequency of BAE, since the BAAE spectral gap is below the BAE spectral gap in the Alfvén continuum. Due to BAAE's low frequency, it is heavily damped by ion kinetic effects,^{35–37} especially when ion temperature (T_i) and electron temperature (T_e) are comparable, which has been verified by simulations.³³ With a strong drive of fast particles, the non-perturbative effect^{38,39} of fast particles should be considered, which will modify radially local dispersion relation³⁴ and thus build up a new wave-particle energy exchange channel. On the other hand, a strong drive will possibly excite multiple Alfvén modes at the same time. Meanwhile, multiple mode co-existence will lead to mode-mode coupling and mode overlap, which may generate cascaded transport that enhances the cross field transport of particle, momentum and energy, therefore degrading the overall system performance. Accordingly, the phenomenon of the co-existence of BAE and BAAE is found at ASDEX²⁹ and NSTX,²⁸ where BAE and BAAE have similar mode numbers and radial location. Especially at NSTX, large particle losses emerge during the co-existence of multiple low frequency Alfvén eigenmodes (AEs), BAE, and BAAE. Besides, recent GTC simulations³⁴ show that dominant mode changes from BAAE in larger tokamak to BAE in small tokamak, due to dependence of wave-particle resonance condition on tokamak size. Considerably, increased fast particle losses due to coupling with RASE and TAE¹⁰ have already been established. Thus, the co-existence of BAE and BAAE will not only provide a new possibility for BAAE excitation, but also provide a typical case to investigate the nonlinear

^{a)}Electronic mail: wzhang@iphy.ac.cn. URL: <https://www.indac.info>.

physics of mode-mode coupling and mode overlap and its impact to particle, moment, and energy transport, which is potentially very important in the future larger tokamak, such as ITER⁴⁰ and DEMO.

In the current work, the co-existence of BAE and BAAE is found in GTC nonlinear simulations, when the pressure gradient of fast electron is big enough. GTC^{41–43} has been successfully applied to the simulation of microturbulence,^{44,45} pressure-driven Alfvén eigenmodes (AEs),^{18,46} current-driven instabilities,^{47,48} and radio frequency waves^{49,50} in fusion plasmas. The wavelet analysis shows that BAAE begins to be observed after BAE is saturated. The mode structure in the linear stage behaves as pure BAE; in the nonlinear stage, the mode structure changes due to overlap of two modes. The phase space structure of the perturbed distribution function of fast electrons shows that the wave-particle resonance region for the BAAE mode appears after BAE saturation and intensity becomes stronger in the later nonlinear time. All these results show that the BAAE and BAE instabilities co-exist in the nonlinear simulations, which provides a new mechanism for BAAE excitation in tokamaks.

This paper is organized as follows: Physical model is presented in Sec. II. Parameters and equilibrium in the simulations are presented in Sec. III. The analysis of the simulation results is in Sec. IV. Section V is the discussion and summary.

II. PHYSICAL MODEL

The gyrokinetic equations⁵¹ are used to describe the plasma of toroidal systems in five-dimensional phase space

$$\frac{d}{dt}f_\alpha(\mathbf{X}, \mu, v_\parallel, t) \equiv \left[\frac{\partial}{\partial t} + \dot{\mathbf{X}} \cdot \nabla + \dot{v}_\parallel \frac{\partial}{\partial v_\parallel} - C_\alpha \right] f_\alpha = 0, \quad (1)$$

$$\dot{\mathbf{X}} = v_\parallel \frac{\mathbf{B}}{B_0} + \mathbf{v}_E + \mathbf{v}_c + \mathbf{v}_g, \quad (2)$$

$$\dot{v}_\parallel = -\frac{1}{m_\alpha B_0} \cdot (\mu \nabla B_0 + Z_\alpha \nabla \phi) - \frac{Z_\alpha}{m_\alpha c} \frac{\partial A_\parallel}{\partial t}, \quad (3)$$

where gyro-center position \mathbf{X} , magnetic moment μ , and parallel velocity v_\parallel are selected as a complete set of independent variables, and the index $\alpha = i, e, fe$ represents the particle species of thermal ion, thermal electron, and fast electron, respectively. Z_α is the particle charge, m_α is the particle mass, C_α is the collisional operator, ϕ and A_\parallel are the electrostatic potential and the vector potential parallel to \mathbf{B}_0 , respectively. Here, $\mathbf{B}_0 \equiv B_0 \mathbf{b}_0$ is the equilibrium magnetic field, $\mathbf{B} = \mathbf{B}_0 + \delta \mathbf{B}$, $\mathbf{B}^* = \mathbf{B}_0^* + \delta \mathbf{B}$, $\mathbf{B}_0^* = \mathbf{B}_0 + (B_0 v_\parallel / \Omega_\alpha) \nabla \times \mathbf{b}_0$, Ω_α is the cyclotron frequency of species α . The compressional component of the magnetic field perturbation is excluded by assuming $\delta B_\parallel = 0$, so that the magnetic field perturbation can be prescribed as $\delta \mathbf{B} = \nabla \times (A_\parallel \mathbf{b}_0)$. The $\mathbf{E} \times \mathbf{B}$ drift \mathbf{v}_E , magnetic curvature drift \mathbf{v}_c , and grad- \mathbf{B} drift \mathbf{v}_g are given by

$$\mathbf{v}_E = \frac{c \mathbf{b}_0 \times \nabla \phi}{B_0}, \quad (4)$$

$$\mathbf{v}_c = \frac{v_\parallel^2}{\Omega_\alpha} \nabla \times \mathbf{b}_0, \quad (5)$$

$$\mathbf{v}_g = -\frac{\mu}{m_\alpha \Omega_\alpha} \mathbf{b}_0 \times \nabla B_0. \quad (6)$$

Since the Larmor radii of electrons are much smaller compared with the characteristic spatial scale of BAE which is of the same order of the thermal ion Larmor radius, the drift-kinetic limit is used for electrons²⁵ for simplicity while the finite Larmor effect is retained for the thermal ion.

For thermal electrons, the transit frequency and bounce frequency are much higher than the BAE frequency, since the mass of electrons is very small. On the other hand, their precession frequency is much lower than the BAE frequency, since their energy is smaller compared with fast electrons. Due to the lack of effective resonance resources, the thermal electrons provide the little kinetic effect to the fast-electron driven BAE mode. For the low frequency mode $\omega \ll k_\parallel v_e$, the thermal electron is further simplified to the fluid-kinetic hybrid model,^{42,52} which consists of a lowest-order adiabatic part and a high-order non-adiabatic part with linear and nonlinear kinetic terms.

In the lowest order of the fluid-kinetic hybrid model, by integrating Eq. (1) in the velocity space and keeping the first-order terms, the fluid continuity equation of thermal electrons can be described by

$$\begin{aligned} \frac{\partial \delta n_e}{\partial t} + B_0 \mathbf{b}_0 \cdot \nabla \left(\frac{n_{0e} \delta u_{\parallel e}}{B_0} \right) + B_0 \mathbf{v}_E \cdot \nabla \left(\frac{n_{0e}}{B_0} \right) \\ - n_{0e} (\mathbf{v}_* + \mathbf{v}_E) \cdot \frac{\nabla B_0}{B_0} = 0, \end{aligned} \quad (7)$$

where $\mathbf{v}_* = \mathbf{b}_0 \times \nabla (\delta P_{e\parallel} + \delta P_{e\perp}) / (n_{0e} m_e \Omega_e)$, $\delta P_{e\parallel} = \int d\mathbf{v} m v_\parallel^2 \delta f_e$, $\delta P_{e\perp} = \int d\mathbf{v} \mu B_0 \delta f_e$, $\delta n_e = \int d\mathbf{v} \delta f_e$ is the perturbed thermal electron density, $n_{0e} \delta u_{\parallel e} = \int d\mathbf{v} v_\parallel \delta f_e$ is the perturbed electron parallel velocity, $n_{0e} = \int d\mathbf{v} f_{0e}$, f_{0e} is the equilibrium distribution function of the thermal electron, and $\delta f_e = f_e - f_{0e}$ is the perturbed distribution function of the thermal electron. Note that $\int d\mathbf{v} = \int_0^{+\infty} d\mu \int_{-\infty}^{+\infty} dv_\parallel 2\pi B_0 / m$.

The perturbed parallel velocity of the thermal electron in the above equation is calculated by inverting the parallel Ampère's law

$$e n_{0e} \delta u_{\parallel e} = \frac{c}{4\pi} \nabla_\perp^2 A_\parallel + Z_i n_{0i} \delta u_{\parallel i} - e n_{0fe} \delta u_{\parallel fe}. \quad (8)$$

The vector potential A_\parallel in the above equation is obtained by using Faraday's law

$$\frac{1}{c} \frac{\partial A_\parallel}{\partial t} = -\mathbf{b}_0 \cdot \nabla \phi - \delta E_\parallel = \mathbf{b}_0 \cdot \nabla (\phi_{eff} - \phi), \quad (9)$$

where an effective scalar potential ϕ_{eff} is defined to represent the parallel electric field,

$$\delta E_\parallel \equiv -\mathbf{b}_0 \cdot \nabla \phi - \frac{1}{c} \frac{\partial A_\parallel}{\partial t} = -\mathbf{b}_0 \cdot \nabla \phi_{eff}.$$

In order to calculate the effective potential ϕ_{eff} , Eq. (1) is expanded in terms of $\delta_m \equiv \omega / (k_\parallel v_e)$ for thermal electrons. The leading order equation reads

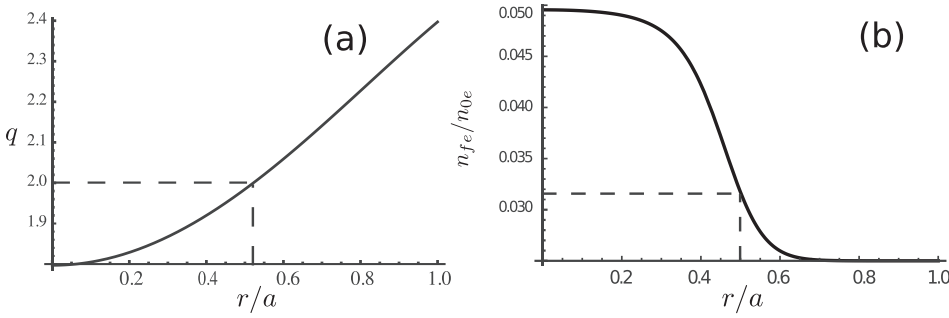


FIG. 1. Safety factor q profile (a) and fast electron density n_{fe} profile (b) in our simulations. The dashed lines correspond to the values around the rational surface $q = 2$.

$$v_{\parallel} \mathbf{b}_0 \cdot \delta f = -v_{\parallel} \frac{\delta B_0}{B_0} \cdot \nabla f_{0e}|_{v_{\perp}} + v_{\parallel} \frac{ef_{0e}}{T_e} \mathbf{b}_0 \cdot \nabla \phi_{eff}. \quad (10)$$

The above Eq. (10) has a solution that can be written as

$$\delta f = \frac{ef_{0e}}{T_e} \phi_{eff} + \left. \frac{\partial f_{0e}}{\partial \psi_0} \right|_{v_{\perp}} \delta \psi, \quad (11)$$

where ψ_0 and $\delta \psi$ are the equilibrium and perturbed poloidal flux, respectively. Equation (11) describes the adiabatic response of thermal electrons, that is, thermal electrons are isothermal along the perturbed magnetic field line, with the Boltzmann response to scalar potential. In deriving Eq. (11), we assume an equilibrium Maxwellian distribution for the parallel velocity with no inhomogeneity along the field line $\mathbf{b}_0 \cdot \nabla f_{0e} = 0$. The notation $\nabla f|_{v_{\perp}}$ means derivation taken at $v_{\perp} = const$ instead of $\mu = const$.

Integrating Eq. (11) over the velocity space, ϕ_{eff} can be expressed as

$$\frac{e\phi_{eff}}{T_e} = \frac{\delta n_e}{n_{0e}} - \frac{\delta \psi}{n_{0e}} \frac{\partial n_{0e}}{\partial \psi_0}. \quad (12)$$

The poloidal flux $\partial \delta \psi / \partial t = -c \partial (\phi_{eff} - \phi) / \partial \alpha_0$, where $\alpha_0 = q(\psi_0)\theta - \zeta$ is the magnetic field line label in terms of the poloidal angle θ and toroidal angle ζ in the magnetic coordinate.

In the lowest order, the pressure term in Eq. (7) is written as

$$\delta P_{e\parallel} = \delta P_{e\perp} = en_{0e} \phi_{eff} + \frac{\partial (n_{0e} T_e)}{\partial \psi_0} \delta \psi. \quad (13)$$

The system can be closed with the gyro-kinetic Poisson's equation⁵³

$$\frac{Z_i^2 n_i}{T_i} (\phi - \tilde{\phi}) = \sum_{\alpha=e,i,fe} Z_{\alpha} \delta n_{\alpha}, \quad (14)$$

where $\tilde{\phi} = \sum_k \phi_k \Gamma_0(k_{\perp}^2 \rho_i^2)$ is the second gyro-phase-averaged electrostatic potential.⁵⁴

III. PARAMETERS AND EQUILIBRIUM

In this work, an equilibrium with a concentric cross-section has been used for simplicity. The safety factor profile [Fig. 1(a)] is $q = 1.797 + 0.8(\psi/\psi_w) - 0.2(\psi/\psi_w)^2$, where ψ is the poloidal flux, $\psi = 0$ is on the magnetic axis, and $\psi = \psi_w$ is at the plasma boundary. The inverse aspect ratio is $\epsilon \equiv a/R_0 = 0.333$ in terms of tokamak minor radius a at wall and on-axis major radius R_0 . The $q=2$ rational surface is located at the local minor radius $r = 0.5a$. The thermal electron density n_{0e} is uniform and the fast electron density [Fig. 1(b)] is $n_{fe} = 0.05n_{0e}(1.0 + 0.25(\tanh((0.2 - \psi/\psi_w)/0.1) - 1.0))$,

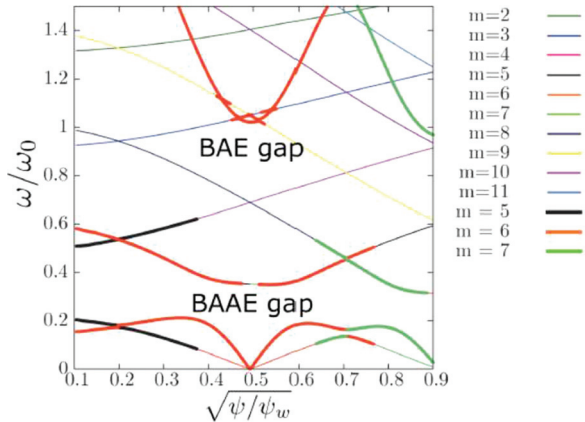


FIG. 2. Alfvénic and acoustic continua for the most unstable toroidal mode $n=3$ are calculated using an eigenvalue code ALCON with poloidal harmonics $m \in [-20, 20]$. The thick lines are the Alfvénic branches and the thin ones are the acoustic branches. The BAE and BAAE spectral gaps are marked.

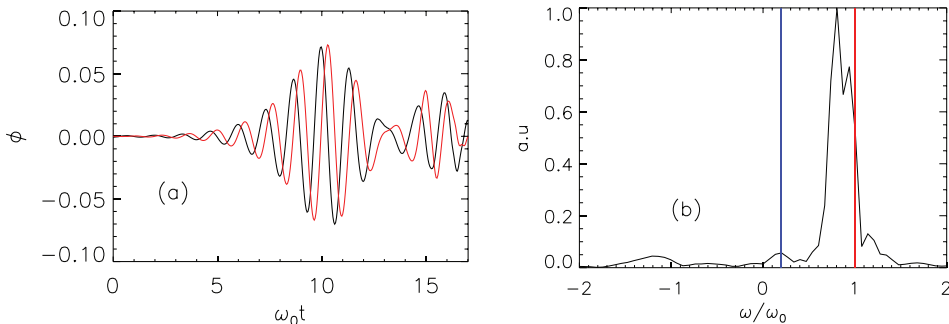


FIG. 3. Time history (a) and frequency spectrum (b). In panel (a), the black line is the real part and the red line is the imaginary part of electrostatic potential. In panel (b), the red line represents ω_0 , and the blue line represents $0.2\omega_0$, which is around the BAAE frequency.

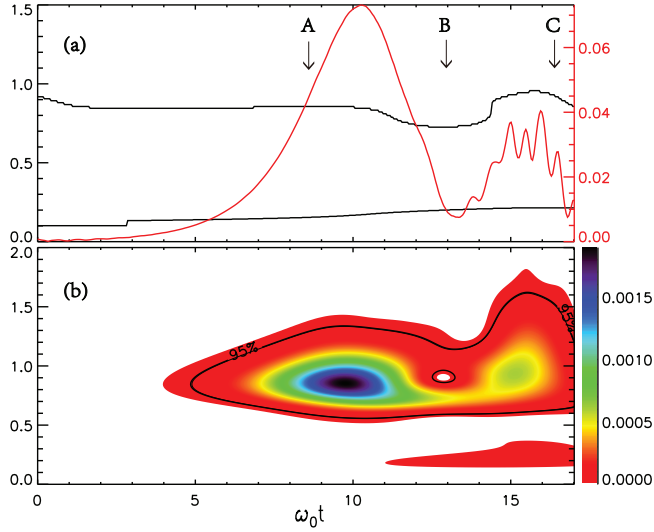


FIG. 4. Time evolution of (a) amplitude of electrostatic potential $|e\phi/T_e|$ and dominant frequency ω (black) of wavelet analysis, and (b) frequency power spectrum. The left axis of panel (a) and (b) is ω/ω_0 . The right axis of panel (a) is in the arbitrary unit. The unit of the power intensity in panel (b) is arbitrary.

so the fast electron density gradient reaches its maximum with $R_0/L_{n_{fe}} = 10$ near the $q=2$ surface, where $L_{n_{fe}}$ is the density gradient scale length of fast electron. The thermal ion density n_{0i} is obtained by the quasi-neutral condition $Z_i n_{0i} = n_{0e} + n_{fe}$, where the thermal ion's charge number is $Z_i = 1$. The thermal plasma temperature is uniform with $T_i = T_e$. The fast electrons

are loaded as a local Maxwellian distribution for simplicity with uniform temperature $T_{fe} = 25T_e$. The thermal plasma's on-axis beta is $\beta = 4\pi n_{0e}(T_e + T_i)/B_0^2 = 0.01436$ with B_0 being the on-axis magnetic field. In the nonlinear simulations, a toroidal mode filter is used to select the most unstable mode $n=3$, which has $k_\theta \rho_i = 0.125$ at the $q=2$ rational surface. Here, $k_\theta = nq/r$ is the poloidal wave-vector, $\rho_i = \sqrt{m_i T_i}/eB_0$ is the thermal ion gyro-radius, $a = 477\rho_i$, and m_i is the ion mass. The parallel wave number is defined as $k_\parallel = (nq - m)/qR$ in terms of major radius R , and it is almost zero at the rational surface. Given all these plasma equilibrium profiles, the frequency of the upper accumulation point of the BAE gap is $\omega_0 = \sqrt{11T_i/2m_i R_0^2} \approx 2.34v_i/R_0$ with the ion thermal velocity $v_i = \sqrt{T_i/m_i}$ and it can correspond to the continuum spectrum (Fig. 2) of the $n=3$ toroidal mode, which is obtained using an eigenvalue code called ALCON⁵⁵ that solves the Alfvén continua with acoustic coupling.

IV. RESULTS AND ANALYSIS

A. History and spectrum

The nonlinear simulation here is an initial value problem and starts with small amplitude random noise. The BAE instability is built-up around the $q=2$ rational surface, and its amplitude oscillates with a real frequency $\omega_{BAE} = 0.85\omega_0$ and grows with a rate $\gamma = 0.11\omega_0$ or $\gamma/\omega_{BAE} = 13\%$, which means that this is a quite strongly driven case. Figure 3(a) shows the time evolution of the $(n, m) = (3, 6)$ mode at the mode rational

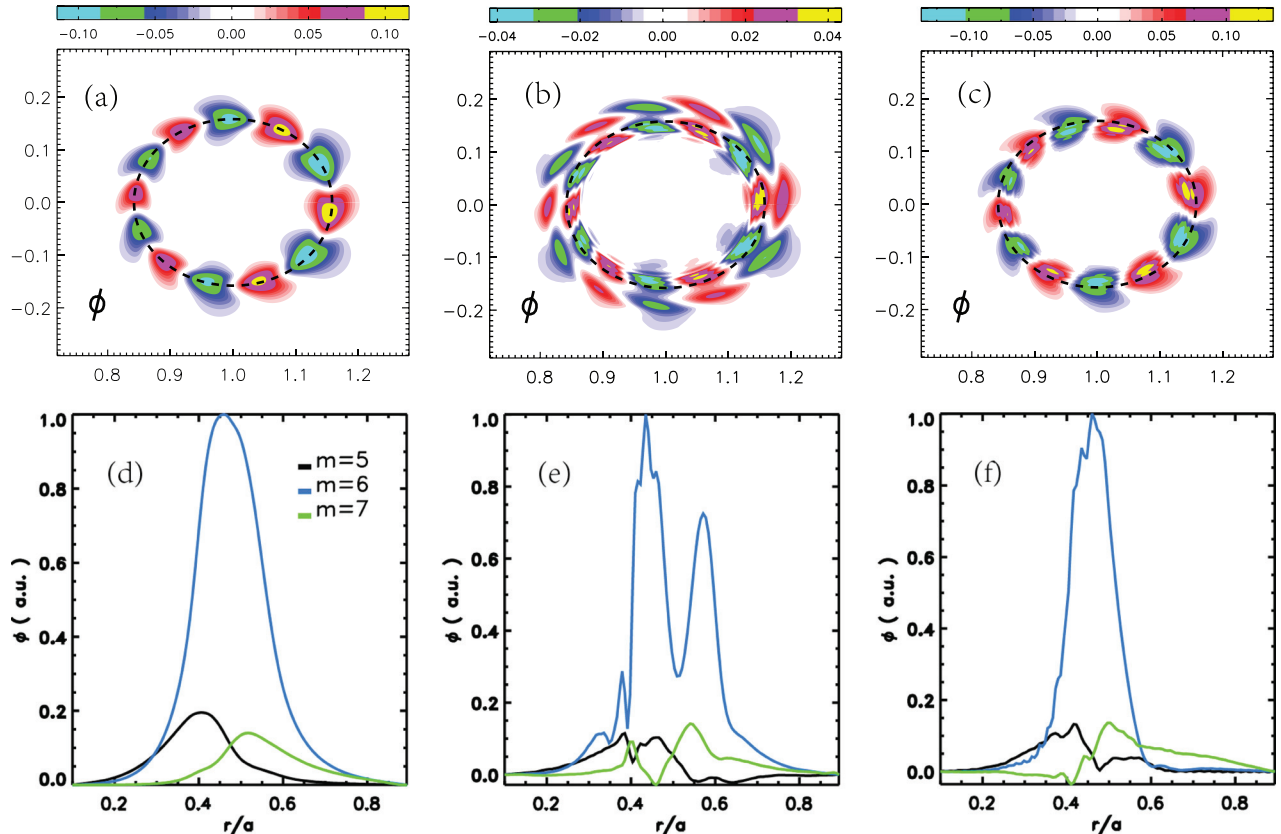


FIG. 5. Poloidal mode structures (a)–(c) and radial profiles (d)–(f) of electrostatic potential $e\phi/T_e$ at three selected typical time points. The dotted circle in panel (a)–(c) is the $q=2$ rational surface. The x axis in panel (a)–(c) is the major radius R/R_0 and the y axis is the vertical distance from the midplane. Time steps for each column from left to right are, respectively, labeled as A–C in Fig. 4.

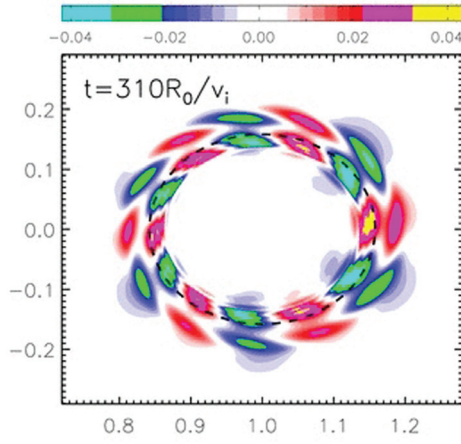


FIG. 6. The evolution of the mode structure. The time point A, B, C corresponds to $200R_0/v_i$, $310R_0/v_i$, $375R_0/v_i$ in the video, respectively. Multimedia view: <http://doi.org/10.1063/1.5004676.1>

surface. The mode reaches a non-regular oscillation state after saturation with its amplitude being $|e\phi/T_e| = 0.075$. The Fourier analysis of the electrostatic potential ϕ in Fig. 3(b) shows that a new branch is found around $\omega \approx 0.2\omega_0$ in the BAAE spectral gap besides the BAE frequency branch. In Fig. 2, the BAAE spectral gap resides in a frequency range which is lower than the BAE spectral gap, and these two modes may locate in the same neighboring region of the rational surface with the same dominant mode number. The wavelet analysis in Fig. 4 shows that there are two frequency regions. The lower region falls in the BAAE spectral gap and the higher region falls in the BAE spectral gap. The BAAE frequency branch is clearly evident right after the BAE instability is saturated. This indicates that BAE and BAAE co-exist in the nonlinear stage of our simulations.

B. Poloidal mode structure

Then, we choose mode structures at three typical time points for further investigation. In the linear stage (point A in Fig. 4), the mode structure has the same poloidal polarization [Fig. 5(d)] as the pure e-BAE.²⁵ In the nonlinear stage (point B in Fig. 4) when BAE's amplitude is nearly minimum in the oscillation process, a new mode branch emerges on the larger radius side of original BAE and it has lower rotation velocity in the θ direction than the BAE branch during the evolution of mode structure (Fig. 6). Therefore, we

can infer that this new branch corresponds to BAAE. In the nonlinear stage (point C in Fig. 4) where BAE's amplitude is predominant again, the mode structure behaves like BAE again.

C. δf and $\delta^2 f$ in (E, λ) space

Generally, the wave-particle resonance condition⁵⁶ for low-frequency waves is $\omega - k_{\parallel}v_{\parallel} - p\omega_t = 0$ for purely passing particles, and $\omega - n\omega_{pre} - p\omega_b = 0$ for deeply trapped particles, where p is an integer number, and ω_t , ω_b , and ω_{pre} , are the guiding center transit, bounce, and precession frequency, respectively. The relative strength of resonances can be inferred from the square of the perturbed distribution function of the fast electron δf_{fe}^2 in the phase space.^{57,58} δf_{fe}^2 is a function of the equilibrium constants of motion (E, λ) , where E is the guiding center kinetic energy and $\lambda = \mu B_0/E$ is a measurement of pitch angle. In the linear stage, only the wave-particle resonance for BAE instability is visible in the δf^2 (Fig. 7(a)) and δf [Fig. 8(a)] plots. In the early nonlinear stage, δf [Fig. 8(b)] does not show BAAE frequency, but δf^2 [Fig. 7(b)] begins to show up the BAAE frequency. In the late nonlinear stage, the resonance region of BAAE is very clear for both δf^2 [Fig. 7(c)] and δf [Fig. 8(c)]. The evolution of the phase space corresponds to wavelet analysis results—the co-existence of BAE and BAAE is found in the nonlinear stage.

V. DISCUSSION AND CONCLUSIONS

In this work, the co-existence phenomenon of BAE and BAAE is found in the nonlinear simulations by using GTC, which provides a new mechanism for BAAE excitation in the presence of strong damping for BAAE in tokamak. In our simulations, the Fourier analysis and wavelet analysis show that after the saturation of BAE, a new frequency branch in the BAAE spectral gap is observed. Next, the poloidal mode structures are investigated. It is found that in the nonlinear stage, a new mode branch emerges on the larger radius side of the original BAE, and this new mode branch has a lower rotation speed in the θ direction than the BAE branch during the evolution of mode structure, which is consistent with the frequency analysis. And the phase space structures of the fast electron perturbed distribution function show that a new resonance region corresponding to BAAE frequency appears after saturation of BAE. Therefore, all the

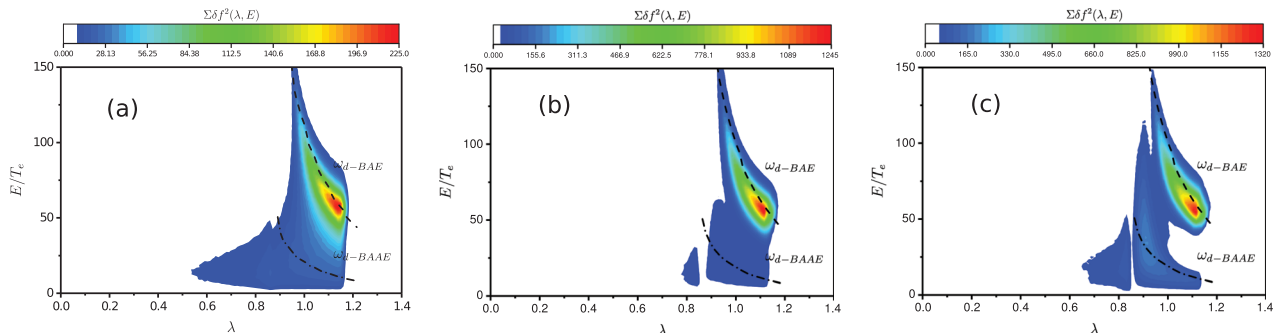


FIG. 7. Phase space (E, λ) structures of δf_{fe}^2 . Dot lines are the wave-particle resonance lines for trapped particles precessional frequency $\omega_{BAE} = \omega_d = n\omega_{pre}$. Dotted-dashed lines are the resonance lines for trapped particles precessional frequency $\omega_{BAAE} = \omega_d = n\omega_{pre}$. Time steps (a)–(c) are labeled as A–C in Fig. 4.

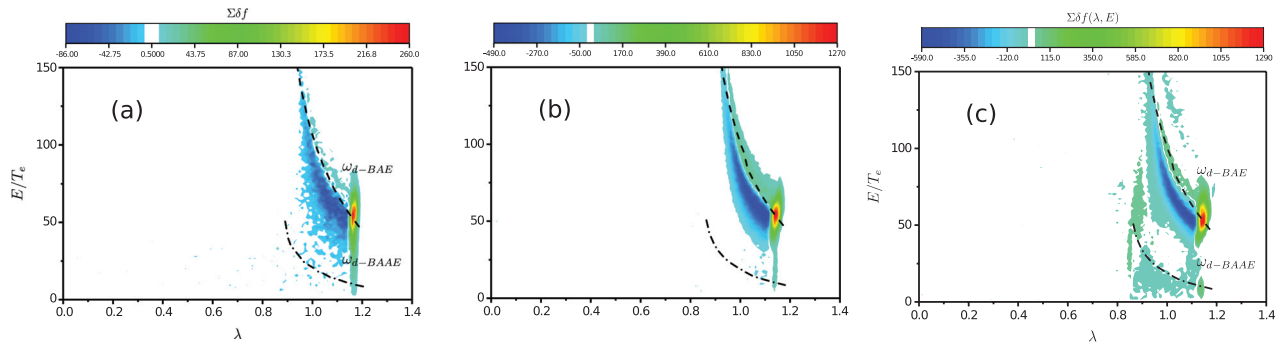


FIG. 8. Phase space (E, λ) structures of δf_{fe} . Dot lines are the wave-particle resonance lines for trapped particles precessional frequency $\omega_{BAE} = \omega_d = n\omega_{pre}$. Dotted-dashed lines are resonance lines for trapped particles precessional frequency $\omega_{BAAE} = \omega_d = n\omega_{pre}$. Time steps (a)–(c) are labeled as A–C in Fig. 4.

above related aspects suggest that the new mode emerging in our nonlinear simulations is a BAAE branch, nonlinearly co-existing with the BAE branch.

In addition, we change the profiles and successfully repeat the co-existence phenomenon, which indicates that there should be a certain physical mechanism. One possible intuitive idea is that the free energy excites BAAE instability after BAE absorbing enough free energy and being saturated. The latter is dominant at the beginning. Furthermore, the co-existence phenomenon is also found in the fast ion driven cases, which is not discussed in this paper. The co-existence of BAE and BAAE has been discussed and investigated through mode structures and phase space structures. This work has setup a useful case that can be used to investigate the nonlinear physics of the mode-mode coupling and mode overlap, which may lead to enhancement of particle, moment, and energy transport and will be presented in the near future.

ACKNOWLEDGMENTS

Authors gratefully acknowledge the useful discussions with Wei Chen, Xuandong Ding, Liming Yu, Yaqi Liu, Huashen Zhang, and Chenxi Zhang. This work was supported by the China National Magnetic Confinement Fusion Science Program under Grant Nos. 2013GB111003 and 2013GB112011, the National Natural Science Foundation of China under Grant Nos. 11675257 and 11675256, the Strategic Priority Research Program of Chinese Academy of Sciences under Grant No. XDB16010300, the Key Research Program of Frontier Science of Chinese Academy of Sciences under Grant No. QYZDJ-SSW-SYS016, and the External Cooperation Program of Chinese Academy of Sciences under Grant No. 112111KYSB20160039. This research used resources of the National Supercomputer Center in Tianjin (NSCC-TJ), the Oak Ridge Leadership Computing Facility at Oak Ridge National Laboratory (OLCF) (DOE Contract No. DE-AC05-00OR22725), and the National Energy Research Scientific Computing Center (NERSC) (DOE Contract No. DE-AC02-05CH11231).

¹G. Y. Fu and J. W. Van Dam, *Phys. Fluids B* **1**, 1949 (1989).

²W. W. Heidbrink, E. J. Strait, M. S. Chu, and A. D. Turnbull, *Phys. Rev. Lett.* **71**, 855 (1993).

³W. W. Heidbrink, E. Ruskov, E. M. Carolipio, J. Fang, M. A. van Zeeland, and R. A. James, *Phys. Plasmas* **6**, 1147 (1999).

⁴H. L. Berk, D. N. Borba, B. N. Breizman, S. D. Pinches, and S. E. Sharapov, *Phys. Rev. Lett.* **87**, 185002 (2001).

⁵B. N. Breizman, H. L. Berk, M. S. Pekker, S. D. Pinches, and S. E. Sharapov, *Phys. Plasmas* **10**, 3649 (2003).

⁶N. N. Gorelenkov, H. L. Berk, E. Fredrickson, S. E. Sharapov, and JET EFDA Contributors, *Phys. Lett. A* **370**, 70 (2007).

⁷N. N. Gorelenkov, H. L. Berk, N. A. Crocker, E. D. Fredrickson, S. Kaye, S. Kubota, H. Park, W. Peebles, S. A. Sabbagh, S. E. Sharapov, D. Stutmat, K. Tritz, F. M. Levinton, H. Yuh, and the NSTX Team and JET EFDA Contributors, *Plasma Phys. Controlled Fusion* **49**, B371 (2007).

⁸E. J. Strait, W. W. Heidbrink, A. D. Turnbull, M. S. Chu, and H. H. Duong, *Nucl. Fusion* **33**, 1849 (1993).

⁹M. Podestà, R. E. Bell, N. A. Crocker, E. D. Fredrickson, N. N. Gorelenkov, W. W. Heidbrink, S. Kubota, B. P. LeBlanc, and H. Yuh, *Nucl. Fusion* **51**, 063035 (2011).

¹⁰M. Garcia-Munoz, I. G. J. Classen, B. Geiger, W. W. Heidbrink, M. A. Van Zeeland, S. Åkäslopmpolo, R. Bilato, V. Bobkov, M. Brambilla, G. D. Conway, S. D. Graça, V. Igochine, P. Lauber, N. Luhmann, M. Maraschek, F. Meo, H. Park, M. Schneller, G. Tardini, and the ASDEX Upgrade Team, *Nucl. Fusion* **51**, 103013 (2011).

¹¹M. S. Chu, J. M. Greene, L. L. Lao, A. D. Turnbull, and M. S. Chance, *Phys. Fluids B* **4**, 3713 (1992).

¹²F. Zonca, L. Chen, and R. A. Santoro, *Plasma Phys. Controlled Fusion* **38**, 2011 (1996).

¹³B. N. Breizman, M. S. Pekker, and S. E. Sharapov, *Phys. Plasmas* **12**, 112506 (2005).

¹⁴R. Nazikian, Z. Chang, E. D. Fredrickson, E. Mazzucato, S. H. Batha, R. Bell, R. Budny, C. E. Bush, C. Z. Cheng, A. Janos, F. Levinton, J. Manickam, D. K. Mansfield, H. K. Park, G. Rewoldt, S. Sabbagh, E. J. Synakowski, W. Tang, G. Taylor, and L. E. Zakharov, *Phys. Plasmas* **3**, 593 (1996).

¹⁵P. Buratti, P. Smeulders, F. Zonca, S. V. Annibaldi, M. D. Benedetti, H. Kroegler, G. Regnoli, O. Tudisco, and the FTU-Team, *Nucl. Fusion* **45**, 1446 (2005).

¹⁶W. Chen, X. Q. Ji, Q. W. Yang, X. T. Ding, Y. Liu, B. B. Feng, Y. Huang, W. Li, Y. Zhou, X. M. Song, L. C. Li, X. R. Duan, and the HL-2A Team, *J. Phys. Soc. Jpn.* **79**, 044501 (2010).

¹⁷C. Nguyen, X. Garbet, R. Sabot, L. G. Eriksson, M. Goniche, P. Maget, V. Basiuk, J. Decker, D. Elbeze, T. A. Huysmans, A. Macor, J. L. Segui, and M. Schneider, *Plasma Phys. Controlled Fusion* **51**, 095002 (2009).

¹⁸H. S. Zhang, Z. Lin, and I. Holod, *Phys. Rev. Lett.* **109**, 025001 (2012).

¹⁹X. Wang, S. Briguglio, L. Chen, C. Di Troia, G. Fogaccia, G. Vlad, and F. Zonca, *Phys. Rev. E* **86**, 045401 (2012).

²⁰W. Park, E. V. Belova, G. Y. Fu, X. Z. Tang, H. R. Strauss, and L. E. Sugiyama, *Phys. Plasmas* **6**, 1796 (1999).

²¹K. L. Wong, M. S. Chu, T. C. Luce, C. C. Petty, P. A. Politzer, R. Prater, L. Chen, R. W. Harvey, M. E. Austin, L. C. Johnson, R. J. La Haye, and R. T. Snider, *Phys. Rev. Lett.* **85**, 996 (2000).

²²X. T. Ding, Y. Liu, G. C. Guo, E. Y. Wang, K. L. Wong, L. W. Yan, J. Q. Dong, J. Y. Cao, Y. Zhou, J. Rao, Y. Yuan, H. Xia, Y. Liu, and the HL-1M Group, *Nucl. Fusion* **42**, 491 (2002).

²³W. Chen, X. T. Ding, Q. W. Yang, Y. Liu, X. Q. Ji, Y. P. Zhang, J. Zhou, G. L. Yuan, H. J. Sun, W. Li, Y. Zhou, Y. Huang, J. Q. Dong, B. B. Feng, X. M. Song, Z. B. Shi, Z. T. Liu, X. Y. Song, L. C. Li, X. R. Duan, Y. Liu, and HL-2A Team, *Phys. Rev. Lett.* **105**, 185004 (2010).

- ²⁴W. Chen, X. T. Ding, Y. Liu, Q. W. Yang, X. Q. Ji, G. L. Yuan, Y. P. Zhang, M. Isobe, Y. B. Dong, Y. Huang, J. Zhou, Y. Zhou, W. Li, B. B. Feng, X. M. Song, J. Q. Dong, Z. B. Shi, X. R. Duan, and HL-2A Team, *Nucl. Fusion* **51**, 063010 (2011).
- ²⁵J. Y. Cheng, W. L. Zhang, Z. Lin, I. Holod, D. Li, Y. Chen, and J. T. Cao, *Phys. Plasmas* **23**, 052504 (2016).
- ²⁶N. N. Gorelenkov, M. A. Van Zeeland, H. L. Berk, N. A. Crocker, D. Darrow, E. Fredrickson, G. Y. Fu, W. W. Heidbrink, J. Menard, and R. Nazikian, *Phys. Plasmas* **16**, 056107 (2009).
- ²⁷L. Chen and F. Zonca, *Phys. Plasmas* **24**, 072511 (2017).
- ²⁸D. S. Darrow, E. D. Fredrickson, N. N. Gorelenkov, A. L. Roquemore, and K. Shinohara, *Nucl. Fusion* **48**, 084004 (2008).
- ²⁹D. Curran, P. Lauber, P. J. Mc Carthy, S. da Graca, V. Igochine, and the ASDEX Upgrade Team, *Plasma Phys. Controlled Fusion* **54**, 055001 (2012).
- ³⁰M. Isobe, K. Ogawa, A. Shimizu, M. Osakabe, S. Kubo, K. Toi, and the LHD Experiment Group, *Plasma Sci. Technol.* **17**, 276 (2015).
- ³¹C. B. Deng, D. L. Brower, B. N. Breizman, D. A. Spong, A. F. Almagri, D. T. Anderson, F. S. B. Anderson, W. X. Ding, W. Guttenfelder, K. M. Likin, and J. N. Talmadge, *Phys. Rev. Lett.* **103**, 025003 (2009).
- ³²S. R. Haskey, B. D. Blackwell, C. Nuhrenberg, A. Konies, J. Bertram, C. Michael, M. J. Hole, and J. Howard, *Plasma Phys. Controlled Fusion* **57**, 095011 (2015).
- ³³H. S. Zhang, Y. Q. Liu, Z. Lin, and W. L. Zhang, *Phys. Plasmas* **23**, 042510 (2016).
- ³⁴Y. Q. Liu, Z. Lin, H. S. Zhang, and W. L. Zhang, *Nucl. Fusion* **57**, 114001 (2017).
- ³⁵F. Zonca, A. Biancalani, I. Chavdarovski, L. Chen, C. Di Troia, and X. Wang, *J. Phys.: Conf. Ser.* **260**, 012022 (2010).
- ³⁶D. Y. Eremin and A. Könies, *Phys. Plasmas* **17**, 012108 (2010).
- ³⁷I. Chavdarovski and F. Zonca, *Phys. Plasmas* **21**, 052506 (2014).
- ³⁸N. N. Gorelenkov and W. W. Heidbrink, *Nucl. Fusion* **42**, 150 (2002).
- ³⁹C. Z. Cheng, N. N. Gorelenkov, and C. T. Hsu, *Nucl. Fusion* **35**, 1639 (1995).
- ⁴⁰See www.iter.org for improvement of device parameters.
- ⁴¹Z. Lin, T. S. Hahm, W. W. Lee, W. M. Tang, and R. B. White, *Science* **281**, 1835 (1998).
- ⁴²I. Holod, W. L. Zhang, Y. Xiao, and Z. Lin, *Phys. Plasmas* **16**, 122307 (2009).
- ⁴³Y. Xiao, I. Holod, Z. X. Wang, Z. Lin, and T. G. Zhang, *Phys. Plasmas* **22**, 022516 (2015).
- ⁴⁴W. L. Zhang, Z. Lin, and L. Chen, *Phys. Rev. Lett.* **101**, 095001 (2008).
- ⁴⁵Y. Xiao and Z. Lin, *Phys. Rev. Lett.* **103**, 085004 (2009).
- ⁴⁶W. L. Zhang, I. Holod, Z. Lin, and Y. Xiao, *Phys. Plasmas* **19**, 022507 (2012).
- ⁴⁷J. McClenaghan, Z. Lin, I. Holod, W. J. Deng, and Z. X. Wang, *Phys. Plasmas* **21**, 122519 (2014).
- ⁴⁸D. J. Liu, W. L. Zhang, J. McClenaghan, J. Q. Wang, and Z. Lin, *Phys. Plasmas* **21**, 122520 (2014).
- ⁴⁹A. Kuley, Z. Lin, J. Bao, X. S. Wei, Y. Xiao, W. L. Zhang, G. Y. Sun, and N. J. Fisch, *Phys. Plasmas* **22**, 102515 (2015).
- ⁵⁰J. Bao, Z. Lin, A. Kuley, and Z. X. Lu, *Plasma Phys. Controlled Fusion* **56**, 095020 (2014).
- ⁵¹A. J. Brizard and T. S. Hahm, *Rev. Mod. Phys.* **79**, 421 (2007).
- ⁵²Z. Lin and L. Chen, *Phys. Plasmas* **8**, 1447 (2001).
- ⁵³W. W. Lee, *J. Comput. Phys.* **72**, 243 (1987).
- ⁵⁴Z. Lin and W. W. Lee, *Phys. Rev. E* **52**, 5646 (1995).
- ⁵⁵W. Deng, Z. Lin, I. Holod, Z. Wang, Y. Xiao, and H. Zhang, *Nucl. Fusion* **52**, 043006 (2012).
- ⁵⁶L. Chen, *J. Geophys. Res.* **104**, 2421, doi:10.1029/1998JA900051 (1999).
- ⁵⁷H. S. Zhang and Z. Lin, *Phys. Plasmas* **17**, 072502 (2010).
- ⁵⁸H. S. Zhang, Z. Lin, W. Deng, I. Holod, Z. X. Wang, Y. Xiao, and W. L. Zhang, *Phys. Plasmas* **20**, 012510 (2013).